Chapter 47
Simulation and Optimization of a Mini Compound Parabolic Collector with a Coaxial Flow System

Dimitrios N. Korres and Christos Tzivanidis

47.1 Introduction

The increasing need for renewable energy sources brinks solar thermal systems at the global foreground by setting them as the main representative of such energy sources. Many different kinds of solar thermal collectors have been set under investigation most of which are the flat plate, the parabolic trough, the compound parabolic, and the evacuated tube collectors (FPCs, PTCs, CPCs, and ETCs).

Korres and Tzivanidis [1] investigated the operation of a flat plate collector with a serpentine flow system through CFD analysis, and they found how the slope of the collector affects the convection inside the gap and as a consequence the thermal performance of the collector. The effects of the plate to cover spacing and the inclination angle at the efficiency of a flat plate collector have been studied from Cooper [2] while an innovative method for calculating the air function inside the gap space of an FPC was applied by Bellos et al. [3]. Subiantoro and Tiow [4] presented analytical models for the top heat losses of an FPC and compared them to CFD analysis conducted with ANSYS.

There are, also, few studies in the subject of compound parabolic and parabolic trough technology. For instance, a mini-compound parabolic collector with a circular absorber and an optically optimized reflector was examined by Korres and Tzivanidis [5, 6], while Korres et al. [7] studied the thermal and the optical performance of a similar collector with a flat receiver. Li et al. [8] compared the thermal efficiency of two different CPCs and concluded that the collector with the lower concentration ratio performs better at high efficiency range while a new flat stationary evacuated CPC was developed and analyzed by Buttinger et al. [9]. Moreover, Antonelli et al. [10] examined the performance of two different CPCs with a

D. N. Korres (✉) · C. Tzivanidis
Mechanical Engineering Department, National Technical University of Athens, Athens, Greece

circular and a flat absorber and found that the first configuration gives greater thermal efficiency in a wide operating range especially at high temperatures. PTCs have, also, been tested by many researchers as far as their thermal and optical performance as well as the heat transfer fluid effect is concerned (Wang et al. [11], Tzivanidis et al. [12]).

The ETC technology is of particular interest since it provides negligible thermal losses, and hence, we can achieve greater thermal performances. There are various different piping systems which could be applied on an ETC the main of which are the heat pipe, the U-pipe, and the coaxial flow configuration. Ayompe and Duffy [13] made a thermal performance analysis of a heat pipe evacuated tube system while Zheng et al. [14] studied on how the emissivity of the back receiver's surface influences the heat losses of a heat pipe application. The U-pipe system has, also, been investigated by Kim and Seo [15] and Pei et al. [16]. Gao et al. [17] put forward a mathematical model so as to describe the thermal behavior of a U-pipe evacuated tube collector, while Liangdong Ma et al. [18] conducted a thermal investigation on a U-type evacuated tube application by analytical method.

As far as the coaxial flow system is concerned, there are not many studies conducted in that field. For instance, Kim et al. [19] evaluated analytically the thermal performance of such a system while Glembin et al. [20] analyzed the impact of the internal thermal coupling between the fluid in the annuli and the fluid in the inner tube of a counter flow ETC on the temperature profile and the thermal efficiency. Zhang et al. [21] examined the performance of a direct flow coaxial evacuated tube collector with and without a heat shield and found that the collector performs better with the shield, while Ataee and Ameri [22] conducted an energy and exergy analysis of a similar collector. Finally, Han et al. [23] used a three-dimensional analytical model to investigate the thermal performance of an all-glass ETC with a coaxial flow conduit.

The aim of this work is to add a different prospect in the field of the coaxial flow ETC analysis through the investigation of the thermal performance and the convection regime of a coaxial flow ETC with a mini-CPC reflector in several operating conditions.

47.2   Collector's Geometry and Data

A coaxial flow evacuated tube collector with a mini-compound parabolic concentrator was designed and simulated in SolidWorks. The geometry and the main dimensions of the collector are depicted on Fig. 47.1.

As Fig. 47.1 suggests, the working medium enters the collector through the inner tube and leaves it via the annulus passage which is formed between the last one and the receiver, while vacuum regime prevails at the interior of the glass tube.

The reflector's geometry is of considerable interest since it optimally cooperates with the absorber tube. More specifically, the focuses and the focal distances of the reflector have not been designed by chance, but the first were deliberately located on
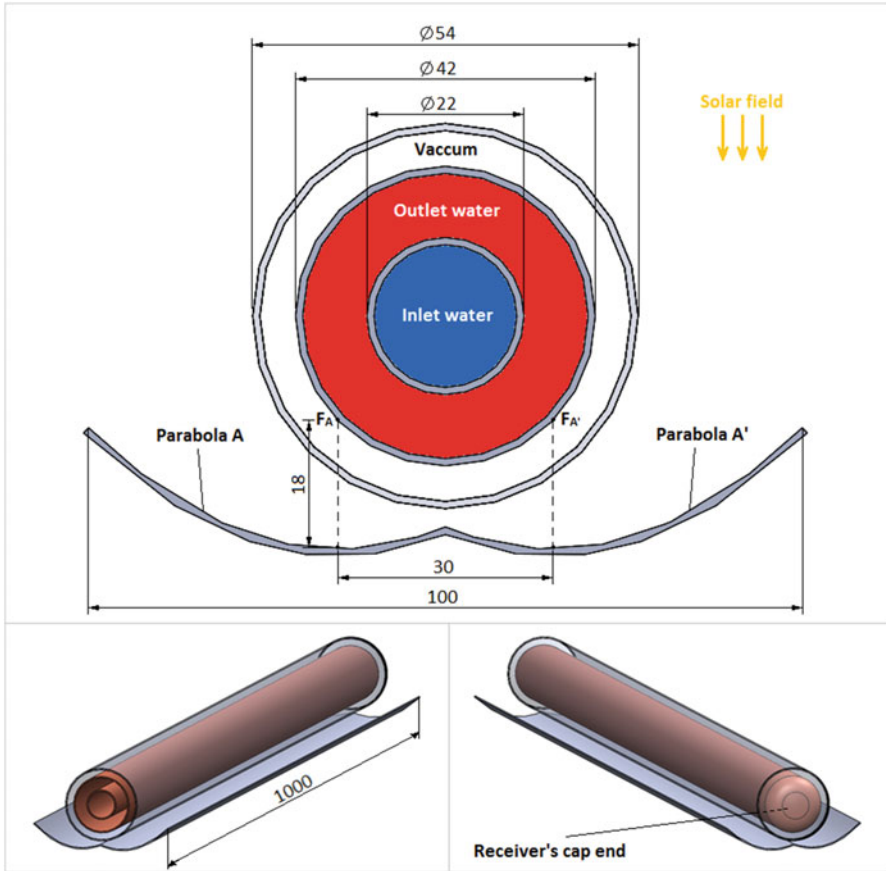
Fig. 47.1 Coaxial evacuated tube collector with a mini-CPC concentrator

Table 47.1 Thermal and optical properties

Component	Material	Thermal properties	Optical properties
Reflector	Aluminum	–	$\rho = 1$
Glass tube	Glass	$\varepsilon_g = 0.88$	$\tau = 1$
Outer tube	Copper	$\varepsilon_p = 0.1$	$\alpha = 0.8$
Inner tube	Copper	–	–

the receiver, while the second were considered to be perpendicular to the aperture plane. This design makes all the perpendicular to the aperture incident solar rays end up on the absorber.

The main characteristics and properties of each component are given bellow in Table 47.1.

Table 47.2 Operating conditions of the collector

Variable	Value	Units
Environment temperature	10	$^\circ$C
Inlet water temperature range	10–100	$^\circ$C
Water mass flow rate	0.004	kg/s
Wind heat transfer coefficient	10	W/m^2/K
Global irradiance	1000	W/m^2

The cover's transmittance and the reflectance of the concentrator take the unit value because we have set all the optical losses on the receiver's outer surface. Hence, the value of 0.8 on the above table does not represent only the absorptance of the receiver tube but also includes the mirror and the glass optical losses. The thickness of all the components is 1 mm.

47.3 Analysis

At this chapter the operating conditions under which our collector is examined are described. Also, the methodology we are going to use so as to analyze the thermal behavior of the collector and to determine the efficiency and the convection regime inside the coaxial conduit is presented.

The collector was tested in ten different inlet water temperatures (T_i) considering that the global irradiance (G_T) is constant and perpendicular to the aperture plane. The operating conditions are given in Table 47.2.

47.3.1 Energy Balance

In Fig. 47.2 a detailed view of the coaxial flow tube and the conditions that prevail in there are depicted while the symbolization we are going to use in our analysis is given too.

Tube energy balance

$$Q_{u,t} = \dot{m} \cdot C_p \cdot (T_{o,t} - T_i) = h_{f,1} \cdot A_{s,1} \cdot (T_{s,1} - T_{f,t}), \qquad (47.1)$$

Cap end energy balance

$$Q_{u,cap} = \dot{m} \cdot C_p \cdot (T_{i,an} - T_{o,t}), \qquad (47.2)$$

Annuli energy balance

$$Q_{u,an} = \dot{m} \cdot C_p \cdot (T_o - T_{i,an}) = h_{f,2} \cdot A_{s,2} \cdot (T_{s,2} - T_{f,an}) - Q_{u,t}, \qquad (47.3)$$
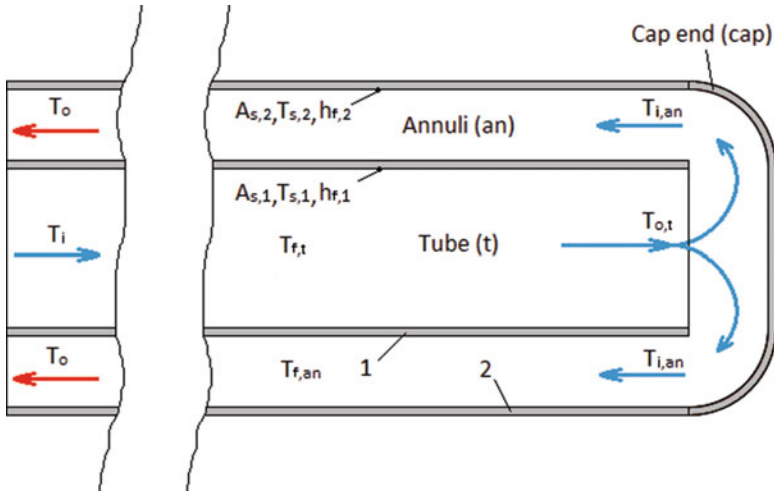
Fig. 47.2 Coaxial flow tube

Total energy balance

$$Q_{u,\text{tot}} = \dot{m} \cdot C_p \cdot (T_o - T_i) = Q_{u,\text{an}} + Q_{u,\text{t}} + Q_{u,\text{cap}}, \tag{47.4}$$

Overall heat losses

$$Q_L = \left[h_w \cdot (T_g - T_\alpha) + \varepsilon_g \cdot \sigma \cdot \left(T_g^4 - T_\alpha^4 \right) \right] \cdot A_{g,o} = \frac{A_p \cdot \sigma \cdot \left(T_p^4 - T_g^4 \right)}{\frac{1}{\varepsilon_p} + \frac{1-\varepsilon_g}{\varepsilon_g} \cdot \frac{D_{p,o}}{D_{g,i}}}, \tag{47.5}$$

Overall heat loss coefficient

$$U_L = \frac{Q_L}{T_p - T_a} \cdot \frac{1}{A_p}, \tag{47.6}$$

Thermal efficiency

$$\eta = \frac{Q_{u,\text{tot}}}{A_a \cdot G_T}, \tag{47.7}$$

Equations (47.1, 47.2, and 47.3) express the useful energy which is conveyed on the water in each specific region of the counter flow conduit, while Eq. (47.4) gives the total water heat gain from the inlet to the outlet of the collector. The overall heat losses, the losses coefficient, and the thermal performance of the system appear on Eqs. 47.5, 47.6, and 47.7, respectively. T_α, T_p, and T_g express the temperatures of the ambient, the absorber, and the glass, respectively.

We have to state that in the specific simulation tool, the bodies which do not have any radiative specification are considered as gray bodies, while thermal radiation emittance is diffusive by default. The second part of Eq. (47.5) holds for such conditions between two long coaxial cylinders (Bergman et al. [24]), so why we used it to calculate the overall heat losses. In addition, the flow inside the tube was considered as laminar due to the low velocity fields.

47.3.2 Efficiency and Losses of the Collector

Figure 47.3 that follows gives the thermal performance of the collector, and the useful energy is conveyed on the heat transfer fluid desperately for each of the three areas of the coaxial tube as a function of the inlet water temperature.

As we can see from Fig. 47.3b, the useful power the water gains at the tube region (Q_{u-tube}) is getting greater as the inlet temperature increases in contrast to the power in the cap (Q_{u-cap}) and the annuli region ($Q_{u-annuli}$). This happens because the difference between the power that passes from the outer tube to the working medium and the annuli useful power become greater as T_i increases. From Fig. 47.3a we observe that the efficiency reduces itself as the inlet water temperature takes greater values. This reduction seems to be quite gently due to the absence of convection inside the glass tube and happens because of the fact that the overall heat losses become greater with T_i as this is depicted in Fig. 47.4.

The main reason that causes this increment in the collector's thermal losses is the receiver's temperature increase which reasonably takes place since the thermal level of the inlet water increases too.
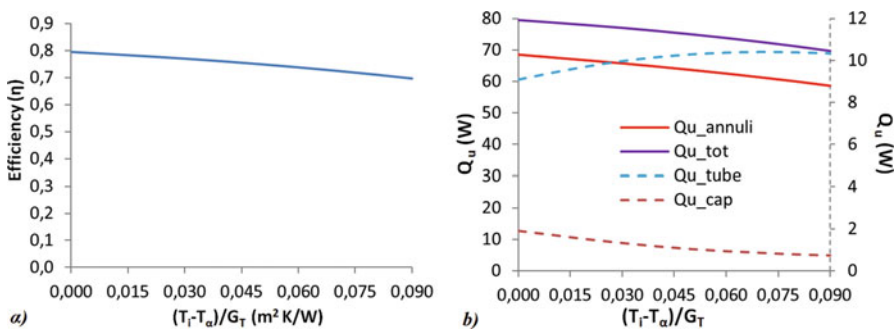

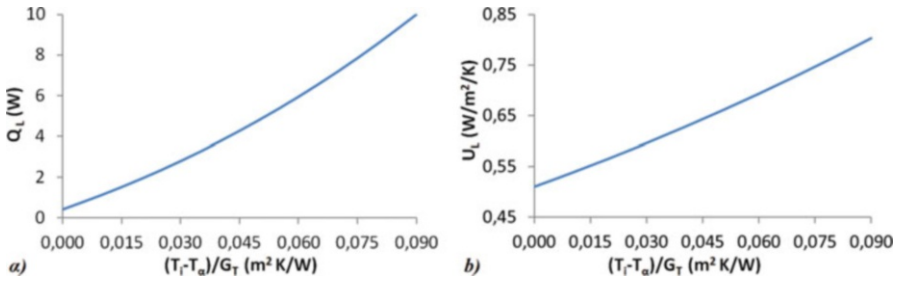**Fig. 47.3** (**a**) Thermal efficiency and (**b**) useful power the water gains totally and separately in each region

Fig. 47.4 (**a**) Overall heat losses and (**b**) overall heat loss coefficient
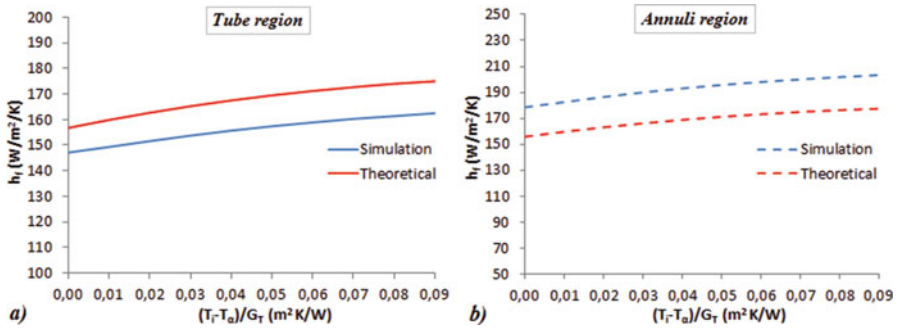

Fig. 47.5 Convective heat transfer coefficient (**a**) in the tube and (**b**) in the annuli

47.3.3 Convection Regime Inside the Coaxial Tube

Here we will determine two different heat transfer coefficients inside the tube. In particular, we are going to calculate the heat transfer coefficient at the inner side of the inner tube and the one at the outer tube (Fig. 47.5). For this calculation, Eqs. 47.1 and 47.3 were solved as below:

$$h_{f,1} = \frac{Q_{u,t}}{A_{s,1} \cdot (T_{s,1} - T_{f,t})}, \tag{47.8}$$

$$h_{f,2} = \frac{Q_{u,an} + Q_{u,t}}{A_{s,2} \cdot (T_{s,2} - T_{f,an})} = \frac{Q_{u,tot} - Q_{u,cap}}{A_{s,2} \cdot (T_{s,2} - T_{f,an})}, \tag{47.9}$$

We, also, validated the specific coefficients through two models of the heat transfer theory. In the tube region, we used the theoretical approach that considers constant surface temperature since the temperature of the inner tube does not change significantly along the flow, while for the annuli area, we considered constant heat

flux conditions since the outer tube is exposed on a constant solar field. These models are described on Eqs. 47.10 and 47.11 that follow:

Tube region

$$h_{f\_T=ct} = \left(3.66 + \frac{0.0668 \cdot Re_{D_{1,i}} \cdot Pr \cdot D_{1,i}/L_t}{1 + 0.04 \cdot \left(Re_{D_{1,i}} \cdot Pr \cdot D_{1,i}/L_t\right)^{2/3}}\right) \cdot \frac{k_f}{D_{1,i}} \qquad (47.10)$$

Annuli region

$$h_{f\_H=ct} = \left(4.364 + \frac{0.036 \cdot Re_{D_{h,an}} \cdot Pr \cdot D_{h,an}/L_t}{1 + 0.0011 \cdot Re_{D_{h,an}} \cdot Pr \cdot D_{h,an}/L_t}\right) \cdot \frac{k_f}{D_{h,an}} \qquad (47.11)$$

where $D_{h,an} = D_{2,i} - D_{1,o}$

The values of Re and Pr were taken for the mean water temperature of each region (from simulation).

It is obvious that the two theoretical curves approach sufficiently the simulation curves. Particularly, there is a mean declination of about 12.6% for the coefficient in the outer tube and 7.5% for the respective at the inner tube. Generally, the convective coefficient increases with T_i because of the thermal conductivity increment.

47.4 Inner Tube Effect

In the specific paragraph, the inner tube's diameter effect on the useful output of the collector is investigated. More specifically, we are going to apply seven different inner diameters of the inner tube (5, 10, 15, 20, 25, 30, and 35 mm) and make a comparison among them in order to determine the best choice. We should mention that for the particular investigation, we removed the glass tube and considered that the outer tube is exposed directly on the environment conditions Table 47.2 suggests. This was done because the examined modifications do not affect significantly the evacuated configuration. Next, a comprehensive table (Table 47.3) which

Table 47.3 Collector's performance and maximum possible efficiency increase dependent on the inner tube diameter and the inlet water temperature

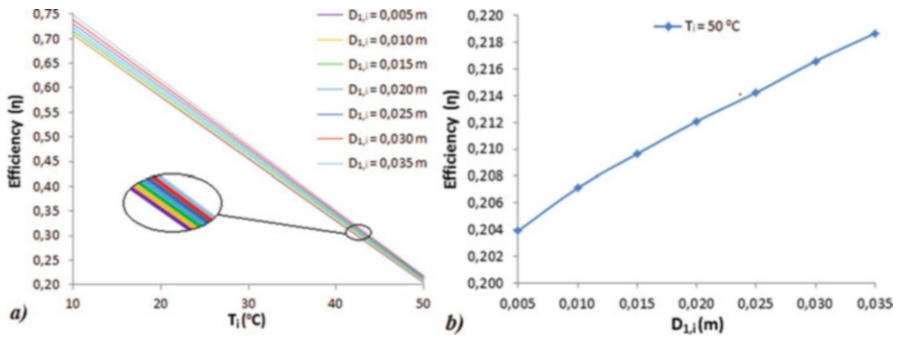| η (%)		$D_{1,i}$ (m)							$\delta\eta_{max}$ (%)
		0.005	0.010	0.015	0.020	0.025	0.030	0.035	
T_i (°C)	10	70.81	70.86	71.51	72.22	72.99	73.84	74.83	5.7
	20	58.19	58.36	58.99	59.43	60.14	60.93	61.70	6.0
	30	45.52	45.84	46.37	46.88	47.37	47.89	48.44	6.4
	40	32.99	33.36	33.79	33.83	34.34	34.93	35.30	7.0
	50	20.39	20.71	20.97	21.21	21.42	21.66	21.87	7.2

Fig. 47.6 Efficiency of the collector dependent on (**a**) $D_{1,i}$ and T_i and (**b**) $D_{1,i}$ for $T_i = 50\,°C$

presents the collector's efficiency and the maximum possible increase of it in each examined case is given.

As we can see from Table 47.3, the collector's efficiency increases as the inner tube approaches the outer one while decreases with T_i because the overall heat losses become greater. The maximum possible performance increment is presented in the last column of Table 47.3 and expresses how much could the efficiency of the collector increase going directly from the worst to the best diameter scenario. So, according to Table 47.3, we have a significant change on the efficiency for all the examined inlet water temperatures by changing the inner tube's inner diameter value from 5 mm to 35 mm. A briefly depiction of the above table is presented bellow on Fig. 47.6 in order to get a more clear view of the problem.

47.5 Allocations and Diagrams

In this chapter a global overview of the collector's thermal behavior is provided via several diagrams and allocations. Figure 47.7 shows the peripheral absorber's temperature and the coaxial tubes' temperature distribution.

As we can observe from Fig. 47.7a, the temperature of the receiver takes its highest values directly at the reflector's parabolas' focal points something that indicates the sufficiency of the simulation.

The receiver's temperature field, on Fig. 47.7b, is depicted as we expected since the temperature increases along the flow. The inner tube seems to follow the receiver's temperature fields something that happens because of the internal thermal coupling between the water and the tubes.

In Fig. 47.8 the bulk average water temperature from the inlet to the outlet of the collector for $T_i = 50\,°C$ and the temperature of the water, the cover, and the glass for each operating point are presented.
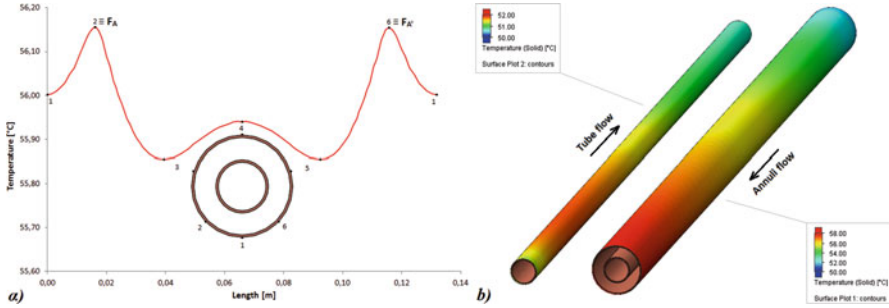
Fig. 47.7 (**a**) Peripheral absorber's temperature and (**b**) delivery and receiver tube wall temperature distribution for $T_i = 50\ °C$
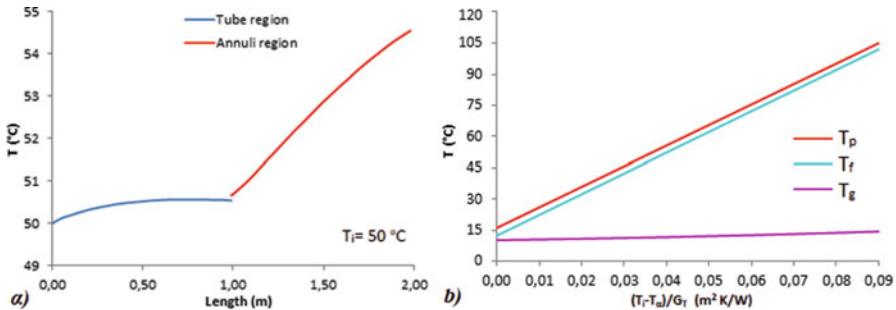

Fig. 47.8 (**a**) Bulk average water temperature along the flow for $T_i = 50\ °C$; (**b**) water, receiver, and glass temperatures

It is obvious that the water temperature increases slightly on the tube region and rapidly on the annuli one since the last one is exposed on the solar heat flux through the outer tube. Regarding Fig. 47.8b the cover temperature is very low compared to the rest temperatures while the divergence between receiver and water temperature is kept almost constant as T_i increases. These two phenomena have to do with the absence of convection at the interior of the glass tube which leads to the elimination of the thermal losses.

The velocity fields are of considerable interest due to the complexity of the flow regime inside the coaxial tube (Fig. 47.9).

The allocations of Fig. 47.9a give a clue about how the flow takes place at the inner tube outfall region. More specifically, as the water exits the inner tube and goes to the annuli, vortices are developed due to the abrupt direction change, something that is depicted clearly at Fig. 47.9b. These vortices seem to behave as a solid body since extremely low velocity fields prevail in them. Hence, Fig. 47.9 gives us an idea on how the main stream of the water is formed by taking into consideration the vortex regime which is an obstacle for the main flow.
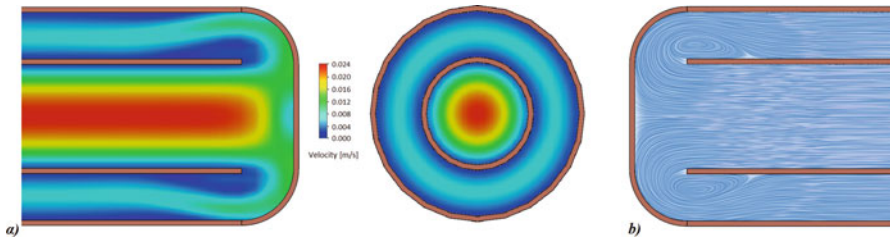
Fig. 47.9 (**a**) Velocity fields inside the coaxial tube for $T_i = 50\,°C$; (**b**) flow streamlines

47.6 Concluding Remarks

In the specific investigation, a coaxial flow ETC with a mini-CPC reflector was examined at several different operating conditions. The thermal performance was determined and found to decrease with the inlet water temperature rise, due to the increment of the overall heat losses. The heat transfer coefficients inside the inner tube and the annuli were both calculated and validated by two theoretical heat transfer models. Particularly, the two respective coefficients diverge from the theoretical values 7.5% and 12.6%, respectively.

In an attempt to examine how the distance between the inner and the outer tube affects the collector's performance, we conducted a relative investigation considering absence of the glass tube. The results were unexpectedly interesting since significant changes in the thermal efficiency were taken place by modifying this diameters' distance. In particular, the thermal performance increases as the inner tube comes closer to the outer one, while this increment becomes greater as the inlet water temperature increases. Specifically, we could have up to 7.2% increment at the thermal performance of the coaxial tube. Hence, the most optimal solution that could provide with high thermal performances that kind of collectors is to bring the coaxial tubes close to each other.

Nomenclature

General Parameters

A	Area (m^2)
C_p	Specific heat (kJ/kg/K)
D	Diameter (m)
G_T	Global irradiance (W/m^2)
h	Convective coefficient ($W/m^2/K$)
k	Thermal conductivity (W/m/K)
L	Length (m)
$\dot{m}$	Mass flow rate (kg/s)
Pr	Prandtl number ($-$)
Q	Heat flux (W)

Re	Reynolds number $(-)$
T	Temperature $(^\circ C)$
U	Thermal transmittance $(W/m^2/K)$

Greek Letters

α	Absorptance $(-)$
ε	Emittance $(-)$
η	Thermal efficiency $(-)$
ρ	Reflectance $(-)$
σ	Boltzmann constant $(W/m^2/K^4)$
τ	Transmittance $(-)$

Subscripts

a	Aperture
α	Environment
an	Annuli
cap	Cap end
f	Water
g	Glass
h	Hydraulic
i	Inlet/inner
L	Overall heat losses
o	Outlet/outer
p	Receiver
s	Walls
t	Tube
tot	Total
u	Useful
w	Wind
1	Inner tube
2	Outer tube without the cap end

References

1. Korres D, Tzivanidis C (2016) Thermal analysis of an entire flat plate collector with a serpentine flow system and determination of the water and air flow and convection regime. In: ECOS 2016: Proceedings of 29th international conference on efficiency, cost, optimization, simulation, and environmental impact of energy systems, Portoroz, Slovenia
2. Cooper PI (1981) The effect of inclination on the heat loss from flat-plate solar collectors. Solar Energy 27:413–420
3. Bellos E, Tzivanidis C, Korres D, Antonopoulos KA (2015) Thermal analysis of a flat plate collector with Solidworks and determination of convection heat coefficient between water and absorber. In: ECOS 2016: Proceedings of 28th international conference on efficiency, cost, optimization, simulation, and environmental impact of energy systems, Pau, France
4. Subiantoro A, Tiow OK (2013) Analytical models for the computation and optimization of single and double glazing flat plate solar collectors with normal and small air gap spacing. Applied Energy 104:392–399

5. Korres D, Tzivanidis C (2017) A new mini-CPC under thermal and optical investigation, IC-SCCE 2016: Renewable Energy, article in press
6. Korres D, Tzivanidis C (2016) Optical and thermal analysis of a new U-type evacuated tube collector with a mini-compound parabolic concentrator and a cylindrical absorber. In: ECOS 2016: Proceedings of 29th international conference on efficiency, cost, optimization, simulation, and environmental impact of energy systems, Portoroz, Slovenia
7. Korres D, Tzivanidis C, Alexopoulos J, Mitsopoulos G (2016) Thermal and optical investigation of a U-type evacuated tube collector with a mini-compound parabolic concentrator and a flat absorber. In: IC-SCCE 2016: Proceedings of 7th international conference from scientific computing to computational engineering, Athens, Greece
8. Li X, Dai YJ, Li Y, Wang RZ (2013) Comparative study on two novel intermediate temperature CPC solar collectors with the U-shape evacuated tubular absorber. Solar Energy 93:220–234
9. Buttinger F, Beikircher T, Pröll M, Schölkopf W (2010) Development of a new flat stationary evacuated CPC-collector for process heat applications. Solar Energy 84:1166–1174
10. Antonelli M, Francesconi M, Di Marco P, Desideri U (2016) Analysis of heat transfer in different CPC solar collectors: a CFD approach. Applied Thermal Engineering 101:479–489
11. Wang Y, Liu Q, Lei J, Jin J (2014) A three-dimensional simulation of a parabolic trough solar collector system using molten salt as heat transfer fluid. Applied Thermal Engineering 70:464–476
12. Tzivanidis C, Bellos E, Korres D, Antonopoulos KA, Mitsopoulos G (2015) Thermal and optical efficiency investigation of a parabolic trough collector. Case Studies in Thermal Engineering 6:226–237
13. Ayompe LM, Duffy A (2013) Thermal performance analysis of a solar water heating system with heat pipe evacuated tube collector using data from a field trial. Solar Energy 90:17–28
14. Zheng H, Xiong J, Su Y, Zhang H (2014) Influence of the receiver's back surface radiative characteristics on the performance of a heat-pipe evacuated-tube solar collector. Applied Energy 116:159–166
15. Kim Y, Seo T (2007) Thermal performances comparisons of the glass evacuated tube solar collectors with shapes of absorber tube. Renewable Energy 32:772–795
16. Pei G, Li G, Zhou X, Ji J, Su Y (2012) Comparative experimental analysis of the thermal performance of evacuated tube solar water heater systems with and without a mini-compound parabolic concentrating (CPC) reflector(C=LT(1)). Energies:911–924
17. Gao Y, Fan R, Zhang XY, AN YJ, Wang MX, Gao YK, Yua Y (2014) Thermal performance and parameter analysis of a U-pipe evacuated solar tube collector. Solar Energy 107:714–727
18. Ma L, Lu Z, Zhang J, Liang R (2010) Thermal performance analysis of the glass evacuated tube solar collector with U-tube. Building and Environment 45:1959–1967
19. Kim JT, Ahn HT, Han H, Kim HT, Chun W (2007) The performance simulation of all-glass vacuum tubes with coaxial fluid conduit. Heat and mass transfer 34:587–597
20. Glembin J, Rockendorf G, ScheurenInternal J (2010) Internal thermal coupling in direct-flow coaxial vacuum tube collectors. Solar Energy 84:1137–1146
21. Zhang X, You S, Ge H, Gao Y, Xu W, Wangb M, He T, Zheng X (2014) Thermal performance of direct-flow coaxial evacuated-tube solar collectors with and without a heat shield. Energy Conversion and Management 84:80–87
22. Ataee S, Ameri M (2015) Energy and exergy analysis of all-glass evacuated solar collector tubes with coaxial fluid conduit. Solar Energy 118:575–591
23. Han H, Kim JT, Ahn HT, Lee SJ (2008) A three-dimensional performance analysis of all-glass vacuum tube with coaxial fluid conduit. Heat and mass transfer 35:589–596
24. Bergman TL, Lavine AS, Incropera FP, Dewitt DP (2011) Fundamentals of heat and mass transfer, 7th edn. John Wiley & Sons Inc, (2011)